JACS
JOURNAL OF THE AMERICAN CHEMICAL SOCIETY
pubs.acs.org/JACS
Article

Quantum Interference-Controlled Conductance Enhancement in Stacked Graphene-like Dimers

Peihui Li,[&] Songjun Hou,[&] Bader Alharbi,[&] Qingqing Wu, Yijian Chen, Li Zhou, Tengyang Gao, Ruihao Li, Lan Yang, Xinyue Chang, Gang Dong, Xunshan Liu, Silvio Decurtins, Shi-Xia Liu,* Wenjing Hong,* Colin J. Lambert,* Chuancheng Jia,* and Xuefeng Guo*

Cite This: *J. Am. Chem. Soc.* 2022, 144, 15689−15697
Read Online

ACCESS | Metrics & More | Article Recommendations | Supporting Information

ABSTRACT: Stacking interactions are of significant importance in the fields of chemistry, biology, and material optoelectronics because they determine the efficiency of charge transfer between molecules and their quantum states. Previous studies have proven that when two monomers are π-stacked in series to form a dimer, the electrical conductance of the dimer is significantly lower than that of the monomer. Here, we present a strong opposite case that when two anthanthrene monomers are π-stacked to form a dimer in a scanning tunneling microscopic break junction, the conductance increases by as much as 25 in comparison with a monomer, which originates from a room-temperature quantum interference. Remarkably, both theory and experiment consistently reveal that this effect can be reversed by changing the connectivity of external electrodes to the monomer core. These results demonstrate that synthetic control of connectivity to molecular cores can be combined with stacking interactions between their π systems to modify and optimize charge transfer between molecules, opening up a wide variety of potential applications ranging from organic optoelectronics and photovoltaics to nanoelectronics and single-molecule electronics.

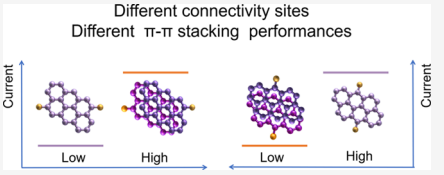

Downloaded via PEKING UNIV on August 31, 2022 at 07:58:06 (UTC).
See https://pubs.acs.org/sharingguidelines for options on how to legitimately share published articles.

INTRODUCTION

Non-covalent stacking interactions, in particular π stacking, are of great significance in the fields of chemistry, biology, and organic optoelectronics.[1−3] They can control charge transfer between molecules, leading to improved efficiency of organic optoelectronic devices, including light-emitting diodes,[4,5] photovoltaic devices,[6,7] and field-effect devices.[8,9] Stacking interactions are also important in vertically stacked two-dimensional (2D) van der Waals (vdW) heterostructures,[10−14] where different stacking configurations, such as AA, AB, or twisted-angle stacking of graphene, can induce unexpected phenomena, including superconductivity,[15] phase transitions,[16] Chern insulators,[17] and Pomeranchuk effect.[18] Graphene-like molecules, such as anthanthrene and pyrene, contain conjugated central units, which were used as models to study intermolecular charge transport and quantum state regulation.[19,20] They have the added advantage that their connections to external electrodes can be engineered with atomic accuracy via chemical synthesis. By varying this connectivity, intramolecular quantum interference (QI) effects can be switched between constructive QI (CQI) and destructive QI (DQI).[20−22] Single-molecule junctions provide an effective platform for studying QI effects in single molecules and dimers.[23,24] In the past two decades, single-molecule experimental measurements[25] and theories[26,27] have revealed a wealth of fundamental knowledge about dimers composed of aromatic or poly-aromatic molecules, including the effects of the electron-transport distance,[28] stacking mode,[29] and stretching process[30] on charge transport. Especially, how to use QI to control the charge and energy flow through such structures[31] and further construct the circuits has attracted extensive attention.[32,33] Recently, it was demonstrated that these quantum effects can be translated into self-assembled molecular layers (SAMs), thereby opening routes to the design of 2D organic materials, whose room-temperature transport properties are controlled by quantum interference. A key feature of SAMs, which is not manifested in single-molecule junctions, is the presence of intermolecular interactions. Therefore, to realize the goal of utilizing quantum-enhanced SAMs in real devices, the interplay between QI and stacking interactions must be clarified. Here, we demonstrate that this interplay could lead to a significant and highly non-classical behavior, even at room temperature.

EXPERIMENTAL METHODS

Experimental Procedures. Gold wire (99.99%, 0.25 mm diameter) was purchased from ZhongNuo Advanced Material (Beijing) Technology Co., Ltd. for the fabrication of the STM tip. The gold tip is obtained by electrochemical corrosion. Substrates were

Received: June 4, 2022
Published: August 5, 2022

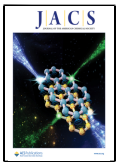

© 2022 American Chemical Society

https://doi.org/10.1021/jacs.2c05909
J. Am. Chem. Soc. 2022, 144, 15689−15697

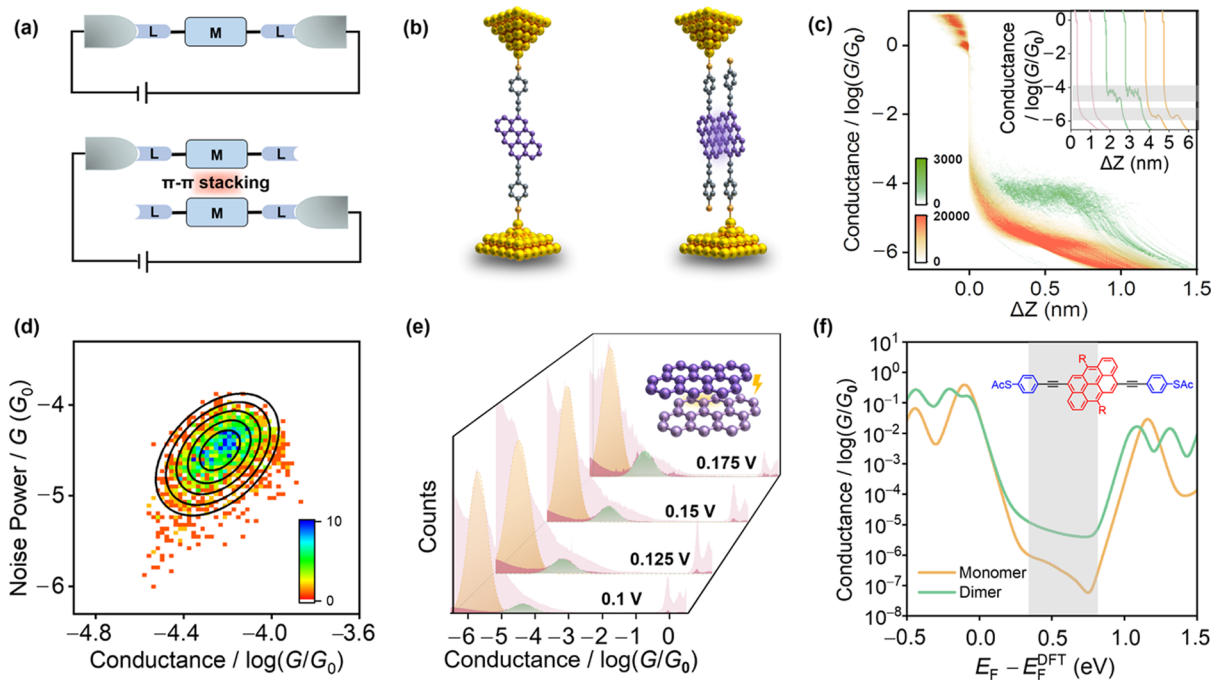

Figure 1. Charge transport through monomer and dimer graphene-like molecules. (a) Schematic representation of circuits with monomer (top) and dimer (bottom). (b) Au-CQI-L-Au junctions measured experimentally using an STM. The left panel shows a single molecule bridging the gap between two gold tips; the right panel shows the junction bridged by a dimer, such that one end group of each monomer is connected to different electrodes through Au-S bonds. (c) 2D conductance-displacement histograms for the junctions constructed from ~4500 individual traces at a bias of 0.1 V. The conductance histograms of the high conductance (green) and the low conductance (yellow) are separated and then plotted in one figure. Inset: typical conductance-displacement traces of background (pink), high conductance (green), and low conductance (yellow). The color scale shows the number of counts normalized to the number of curves included in the histograms. (d) 2D histogram of the normalized noise power versus average conductance for the high conductance state of CQI-L, calculated for 5000 measured traces. (e) One-dimensional (1D) conductance histograms at different potentials of 0.100, 0.125, 0.150, and 0.175 V. Inset: schematic diagram of the electrostatic interaction within the dimer under bias voltages. (f) Theoretical predictions for the conductance of the monomer (yellow) and the dimer (green) of CQI-L molecules as a function of the Fermi energy E_F, with experimentally relevant values of E_F corresponding to the shaded region. The dimer conductance is evaluated by averaging three archetypal stacking patterns, weighted by Boltzmann factors determined by their stacking energies.

prepared by depositing a 10 nm thick chromium film and a 200 nm thick gold film on the N monocrystalline face of a silicon wafer. The target molecules were mixed with 1,2,4-trichlorobenzene (TCB).

In the STM-BJ measurement, the distance between the gold tip and the substrate is controlled by a stepper motor and a piezo stack. Bias voltage is applied between the tip and the substrate, and the current is used as the feedback to control the movement of the gold tip. During the repeating opening (tip retracting) and closing (tip approaching) cycles, the conductance versus displacement traces were collected, and the traces of the opening cycles were used for further analysis. All measurements were carried out at room temperature. Single-molecule conductance measurements were carried out using an Xtech STMBJ, and the data were analyzed by the XMe open-source code (https://github.com/Pilab-XMU/XMe_DataAnalysis).

Theoretical Methods. Geometrical optimizations have been performed by using the DFT code SIESTA,[34] with a generalized gradient approximation GGA functional, a double-ζ polarized basis for other elements, a cutoff energy of 200 Ry, and a 0.02 eV/Å force tolerance. In order to compute their electrical conductance, the molecules were each placed between Au electrodes. For each structure, the transmission coefficient $T(E)$ describing the propagation of electrons of the energy E from the left to the right electrodes was calculated using Gollum code,[35] which combines the mean-field Hamiltonian and overlap matrices of the DFT code SIESTA with Landauer-based quantum transport theory using the expression

$$T(E) = Tr[\Gamma_L(E)G_r(E)\Gamma_R(E)G_r^{\dagger}(E)]$$

where $\Gamma_{L,R}(E) = i(\Sigma_{L,R}(E) - \Sigma_{L,R}{}^{\dagger}(E))/2$, $G_r(E) = (g^{-1} - \Sigma_L - \Sigma_R)^{-1}$, g is the Green's function of the isolated molecule, $\Gamma_{L,R}$ determines the widths of transmission resonances, $\Sigma_{L,R}(E)$ are the self-energies describing the contact between the molecule and left (L) and right (R) electrodes, and G_r is the retarded Green's function of the molecule in the presence of the electrodes. The room temperature conductance was extracted from the transmission spectrum and evaluated by the following formulae

$$G = G_0 \int dE T(E)\left(-\frac{df(E)}{dE}\right)$$

where $G_0 = 2e^2/h$ is the conductance quantum, h is Planck's constant, e is the charge of a proton, and $f(E)$ is the Fermi function.

RESULTS AND DISCUSSION

Charge Transport through Graphene-like Molecules.

Figure 1a (lower) and Figure 1b (right) show the strategies of how electrical current flows sequentially from one monomer to the dimer via π-π stacking. Classically, the electrical conductance of two identical conductors in series is lower than that of a single conductor (Figure 1a). Correspondingly, previous studies revealed that the conductance of a dimer is generally lower than that of the corresponding monomer, even in the presence of quantum effects.[3,30,36,37] For example, for an oligo-phenylene-ethynylene (OPE3) π-conjugated molecule system, periodic reductions in dimer conductance induced by mechanically controlled quantum interference have been

https://doi.org/10.1021/jacs.2c05909
J. Am. Chem. Soc. 2022, 144, 15689−15697

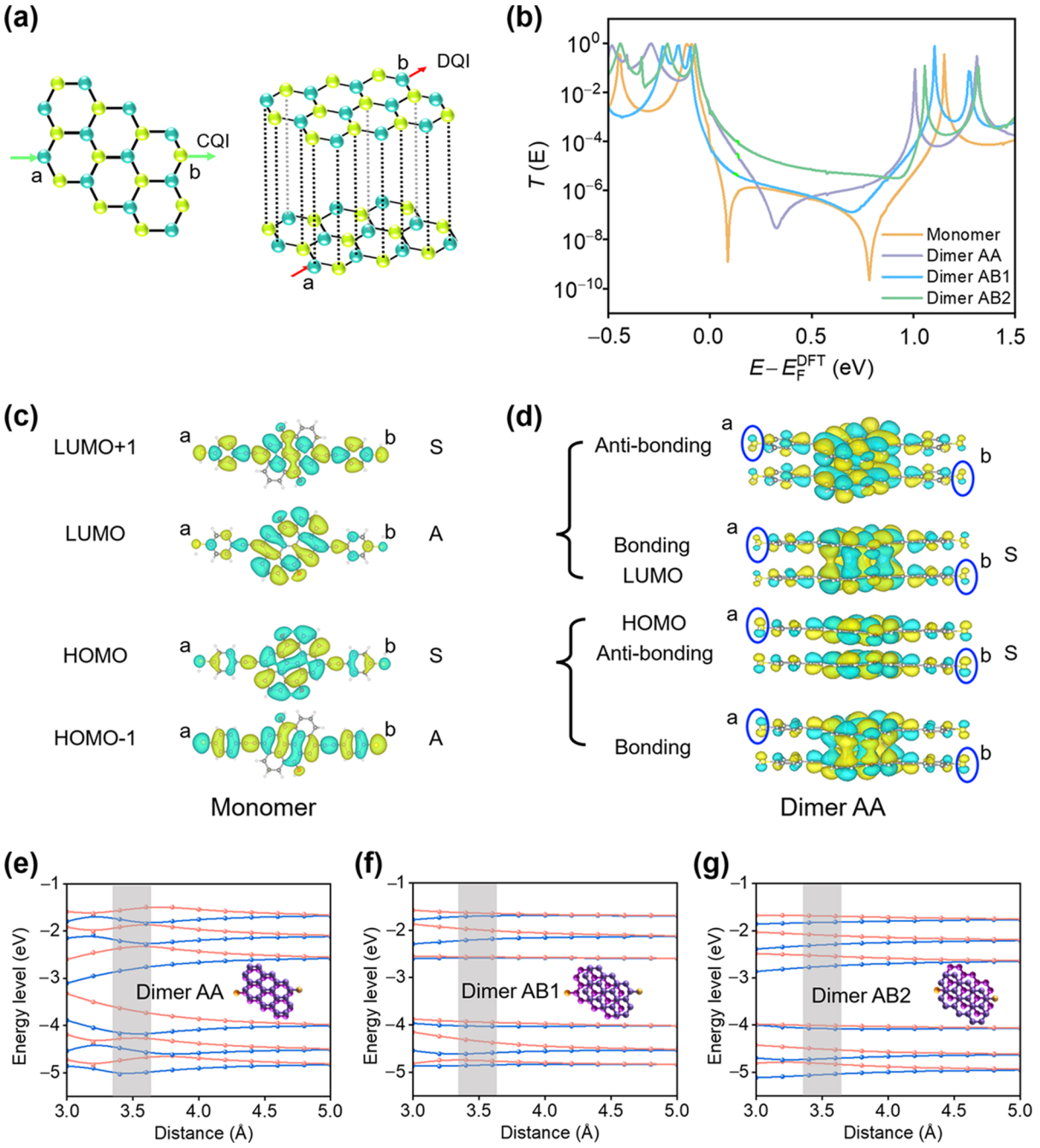

Figure 2. Mechanism of the enhanced conductance in a stacked dimer. (a) Transport properties of monomer and dimer anthanthrenes. Left panel: a lattice representing the CQI-L monomer (CQI, green arrows) and the corresponding AA-stacked dimer (DQI, red arrows). The character of the bipartite property of benzene is denoted by the yellow and green points; that is, the yellow site is only connected to the green site and vice versa. (b) Transmission coefficients as a function of electron energy for the CQI-L monomer and dimers with AA, AB1, and AB2 stacking. (c) Frontier molecular orbitals of the CQI-L monomer: HOMO − 1, HOMO, LUMO, and LUMO + 1. S (i.e., symmetric) denotes the same color for the two opposite ends of each orbital, and A (i.e., anti-symmetric) indicates different colors at opposite ends. (d) HOMO and LUMO splitting to form bonding and anti-bonding pairs induced by dimerization. The new LUMO possesses the same color (S) at the injecting and collecting ends (guided by blue circles) opposite to the case in the LUMO of the monomer. The new HOMO displays the same color at the two ends, as in the case in the monomer HOMO. (e−g) Evolution of energy levels from HOMO − 2 to LUMO + 2 as a function of distance between the two monomers in the vertical direction for AA, AB1, and AB2 stacking. Vertical means the direction perpendicular to the paper, that is, the distance between the graphene-like planes. The expected distance in experiments is guided by the gray windows.

observed.[36] It is worth noting that the charge transport mechanism of the dimer and the conductance mechanism of classical electrical circuits are quite different. In this study, we investigate charge transport through a graphene-like dimer (Figure 1b) using a combination of the scanning tunneling microscope break junction (STM-BJ) technique[38−40] and density functional theory (DFT)[35] and demonstrate that depending on the specific QI pattern and stacking configuration, the conductance of the dimer can be ∼25 times higher than that of the monomer. This abnormal conductance increase in our system is different from conductance superposition in single-molecule circuits with parallel paths.[41]

https://doi.org/10.1021/jacs.2c05909
J. Am. Chem. Soc. 2022, 144, 15689−15697

The chosen monomer (Figure 1b left) is denoted as CQI-L (a constructive QI molecule with a relatively low conductance) and is shown in the inset of Figure 1f and Figure S1-1a. It is composed of a graphene-like anthanthrene core with acetylthiol terminal groups,[19] which bind the molecule to external electrodes. When current is injected and collected via the triple bonds connected to the anthanthrene core, as depicted in Figure 1f, this CQI-L monomer exhibits CQI as shown in a previous study,[20] but with a relatively low (L) conductance. Using the STM-BJ technique, the conductance of a molecular junction is repeatedly measured as a function of tip-substrate displacement to generate conductance versus displacement traces. Specifically, the molecular junctions are formed and broken in a TCB solution. This allows the possibility of either a single monomer bridging the gap between both tips, or two different monomers binding to different tips, so that current flows from one electrode to the other via π-π stacking. To improve the junction formation probability, the acetyl protecting groups of the molecule are deprotected by 1,8-diazabicyclo[5.4.0]undec-7-ene (DBU) to form covalent Au-S bonds, with pre-assembly for 24 h. The results of both X-ray photoelectron spectroscopy (XPS) (Figure S2) and comparative STM experiments without pre-assembly (Figure S3) confirm that an SAM of CQI-L is successfully assembled on gold films with pre-assembly.

Typical individual traces for the junctions under 0.1 V bias are presented in Figure 1c, insert. The conductance features at integer multiples of G_0 ($G_0 = 2e^2/h$) can be observed, as well as the features below G_0 at specific molecular values. The pink traces show the tunneling decay after the rupture of a Au atomic contact in the pure solvent, while the conductance plateaus corresponding to the molecular conductance are found in solution with target molecules. Hundreds to thousands of such conductance traces are used to construct the conductance histograms. Figure 1c presents the two-dimensional (2D) conductance-displacement histograms of a molecule CQI-L (Figure S4). A low conductance peak at $\sim 2.0 \times 10^{-6}$ G_0 ($\approx$0.16 nS) corresponding to the Gaussian fitting peak can be observed. This corresponds to the most-probable conductance of a single CQI-L molecule as reported in previous work.[19] In addition to this monomer conductance peak, a second conductance peak at $\sim 5.0 \times 10^{-5}$ G_0 ($\approx$3.9 nS) (Figure 1c) can be observed, which is more than 25 times higher than the conductance of the monomer. This enhancement is consistent with our theoretical prediction as shown in Figure 1f.

To further determine the cause of the high conductance state, flicker noise analysis is performed to evaluate the transmission coupling. All flicker noise analysis focuses on the high conductance state of the molecular junctions. In light of previous reports,[39,42,43] the noise power scaling as $G^{2.0}$ is indicative of through-space coupling, while $G^{1.0}$ indicates through-bond coupling. Figure 1d shows a 2D histogram of the noise power spectral density (PSD) attributed to the high conductance state of the molecule CQI-L (see the Supporting Information for more details, Figure S6-1 and Figure S6-2). The noise power scales as about $G^{2.0}$, which means that charge transport resulting in the high conductance is dominated by through-space coupling transmission. Thus, this high conductance state of the molecule CQI-L can be attributed to π-stacked dimers (Figure 1b right), in agreement with theoretical simulations presented in Figure 1f, which shows the conductance versus the Fermi energy E_F (relative to the DFT-predicted Fermi energy E_F^{DFT}) for the monomer (yellow curve) and dimer (green curve). Previous work[19] has shown that experimentally relevant values of $E_F - E_F^{DFT}$ correspond to the values near the middle of the HOMO-LUMO gap, indicated by the shaded region, where the dimer to monomer conductance ratio varies from approximately 13 to 70. The high conductance state of π-stacked dimers is further confirmed by using bias-voltage-dependent experiments. Specifically, previous studies have shown that since the electric field can increase the intermolecular attraction, promoting dimer formation in general, the intensity of the conductance peak associated with dimer formation will increase with bias.[44] Figure 1e shows one-dimensional (1D) conductance histograms of the molecule CQI-L measured at different potentials of 0.100, 0.125, 0.150, and 0.175 V. It can be observed that the relative ratio of the high conductance state to the low conductance state increases with increasing bias voltage, as expected for a high conductance state that originates from bimolecular interactions.[44] It is worth noting that although the relative ratio of the high conductance state to the low conductance state increases, the low conductance feature is statistically much more prevalent than the high conductance feature. This is because the low conductance feature is assigned to the monomer with intrinsic characteristics, while the high conductance originates from the dimer with a specific stacking mode. Next, we focus on another key factor: plateau length. As shown in a previous work, the plateau length of the conductance state is correlated with the molecular length.[45] Here, the plateau length is defined from $\sim 10^{-0.3}$ G_0 down to $\sim 10^{-0.2}$ G_0, lower than the specific conductance peak, as shown in Figure S5-2. The high-conductance and low-conductance lengths are consistent with the presence of dimers and monomers, respectively (Figure S5-2). This is also consistent with the theoretical prediction that the most stable structure of the dimer state corresponds to AB stacking (Figure S7).

Theoretical Analysis of the Enhanced Conductance in Dimers. This highly non-classical behavior is a consequence of room-temperature QI between the π systems of the stacked monomers. QI effects in the monomers are primarily driven by the bipartite character of the anthanthrene core. As shown in the left panel of Figure 2a, in a simple Hückel (i.e., tight-binding) description of charge transport through the π system, carbon atoms can be regarded as "green" or "yellow" sites, with green sites connected to yellow sites only and vice versa. As discussed elsewhere,[20,37,46−49] when an electron is injected through a green site (such as site a) and collected via a yellow site (such as site b), or vice versa, this can lead to CQI. In contrast, DQI is induced when an electron is injected through a green site and collected via a green site (or injected through a yellow site and collected via a yellow site) (for more details, see the discussion of a benzene dimer and magic ratio theory in the Supporting Information, Figures S8−S9 and Tables S1−S2). Therefore, the path from site a to site b indicated by green arrows corresponds to CQI.

To highlight the interplay between QI and stacking interactions, we consider a simple tight binding model, in which only nearest-neighbor couplings are present. In this case, the AA stacked dimer is still a bipartite lattice as indicated by the yellow and green sites in the right panel of Figure 2a. However, the path indicated by the red arrows from site a of the lower monomer to site b of the upper monomer now corresponds to DQI since the collecting and injecting sites are both green. Consequently, for AA stacking, the conductance of

https://doi.org/10.1021/jacs.2c05909
J. Am. Chem. Soc. 2022, 144, 15689−15697

the dimer is expected to be lower than that of the monomer, as has been reported in the literature.[36,37] In a real experiment, many stacking configurations are possible and AA stacking is not the most favored. Therefore, although this simple example is useful for illustrating the interplay between QI and stacking interactions, it is not representative of our experimental measurements and DFT modeling, which reveal the fact that the most-probable conductance of the anthanthrene dimer is a factor of 25 higher than that of the monomer.

To elucidate the origin of this highly non-classical conductance increase, we calculated the transmission coefficient $T(E)$ describing electrons of the energy E passing through the molecular junctions shown in Figure 1b, using DFT in combination with the quantum transport code Gollum.[35] To describe the transmission through the dimer, three archetypal stacking patterns were considered, denoted as AA, AB1, and AB2 (Figure S7). As shown in Figure 2b, the resulting transmission coefficients near the middle of the HOMO-LUMO gap are sensitive to the nature of the stacking mode. For AB2 stacking, the mid-gap transmission coefficient of the dimer (green curve) is significantly higher than that of the monomer (yellow curve). For AB1 stacking, it is almost identical with that of the monomer, whereas for AA stacking, it may be higher or lower, depending on the energy E. The ground state energies of fully relaxed AB1 and AB2 stacking are lower than that of AA stacking by ∼0.48 and ∼0.52 eV, respectively (Figure S7), meaning that AA is extremely rare at room temperature and the Boltzmann distribution weighted conductance is dominated by the conductance of AB2 stacked dimers (Figure 1f).

To understand the shapes of these curves, we first consider the monomer. According to an orbital product rule,[50,51] the contribution from each molecular orbital to charge transport depends on the colors of the orbitals on sites a and b, which are connected with the electrodes. For the monomer shown in Figure 2c, the highest occupied molecular orbit (HOMO) is the same color denoted by (S) at the two ends (a and b), while the lowest unoccupied molecular orbit (LUMO) has different signs (A) at the two ends, leading to CQI revealed by the flat mid-gap transmission curve (yellow in Figure 2b). However, since LUMO + 1 and LUMO have different symmetries (i.e., colors at the two ends), they interfere destructively at energies in the HOMO-LUMO gap just below the LUMO, leading to an anti-resonance in the yellow curve. Similarly, an anti-resonance appears just above the HOMO due to the different symmetries of HOMO − 1 and HOMO.

To understand the shapes of the dimer transmission curves, we first consider the case of AA stacking, for which CQI in a monomer switches to DQI in the dimer (as demonstrated in the illustrative case of stacked benzenes discussed in the Supporting Information, Figures S8−S9 and Tables S1−S2), leading to a transmission dip at $E - E_F^{DFT} = 0.3$ eV in the purple curve in Figure 2b. This mechanism can also be understood by examining the molecular orbitals of the dimer. When two monomers approach each other and the distance between the two monomers decreases, the π-π interaction causes the monomer orbitals to form pairs of bonding and anti-bonding orbitals of the dimer. As shown in Figure 2d, the new LUMO and the new HOMO of the dimer both possess the same color (S) at the injecting and collecting ends (indicated by blue circles), which leads to a DQI in the dimer.

For each of the three archetypal stacking patterns, the evolution of the energy levels of the dimer, as a function of the vertical distance between the monomers, is shown in Figure 2e−g. This shows that as the distance decreases from 5 toward 3 Å, the pairs of degenerate energy levels (one from each monomer) split. For AA stacking, the inter-monomer coupling matrix is almost equal to the unit matrix. Therefore, since monomer orbitals are orthogonal, there is non-zero coupling only between each orbital on one monomer and its partner orbital on the other monomer. Consequently, monomer levels evolve into pairs of dimer levels and the spectrum of the AA-stacked dimer exhibits only a slight level repulsion. For example, the LUMO + 1, LUMO + 2, LUMO + 3, and LUMO + 4 are at a distance around 3.6 Å. For AA stacking, the DQI feature in the HOMO-LUMO gap of Figure 2b lowers the conductance in spite of the strong couplings between each pair of the energy levels. For the AB1-stacked dimer, Figure 2f shows that the HOMO and LUMO are almost degenerate indicating a very weak coupling between the two HOMOs and two LUMOs in the dimer even at the optimal distance around 3.5 Å. Consequently, the DQI features just below the LUMO and just above the HOMO (in the yellow curve) are no longer present in the blue transmission curve of Figure 2b. In contrast, for the AB2-stacked dimer, Figure 2g shows that the HOMOs are weakly coupled and LUMOs are strongly coupled (Figure 2g). Consequently, the DQI dip is removed since the weakly coupled HOMOs make almost no contribution to the transport. On the other hand, the stronger coupling between the LUMOs leads to a higher value for the green transmission curve in Figure 2b.

One might propose another explanation in which the dimer anthanthrenes are bound to two electrodes with two thiol groups connected to the electrode on each side, such as the example shown in the bottom panel of Figure S10a. However, even though the superposition effect is considered, the significant change of the stacking pattern during the relaxation process results in an enhancement of about 3.1 times, which is much smaller.

It is interesting to note that the high conductance state is not simply confined to AB2 stacking. Starting from the AB2 dimer and shifting or rotating the top monomer, Figure S11 shows that the higher conductance of the dimer persists when the shifting distance is in the range of 2.0 Å or the degree of rotation is in the range of 15.0°. This broadening characteristic of the high conductance state can also be observed in the experimental results (Figure S12), which reveal that the full width at half-maximum (FWHM) obtained by Gaussian fitting for the high conductance state is also wider than that of the low conductance state (Figure S5).

It is worthwhile to explore the universality of the non-classical enhancement, especially the impact of the central size of graphene-like fragments. Since there are a lot of variations in the connectivity and topology, extensive studies need to be done to clarify this point. Here, in Section 13 of the Supporting Information, we only discuss some classical cases that graphene fragment models consist of 1, 2, 4, 6, and 8 benzene rings as central cores (Figure S13). The results show that for all molecules 1, 2, 4, 6, and 8, such non-classical enhancement exists, and ratios of about 5, 12, 180, 20, and 15 are obtained, respectively.

Charge Transport of the Comparative System. The above-enhanced conductance of the dimer in comparison with the monomer can be controlled by varying the connectivity of the anthanthrene core to the electrodes. To illustrate this feature, consider the monomer shown in Figure 3a (left), in

https://doi.org/10.1021/jacs.2c05909
J. Am. Chem. Soc. 2022, 144, 15689−15697

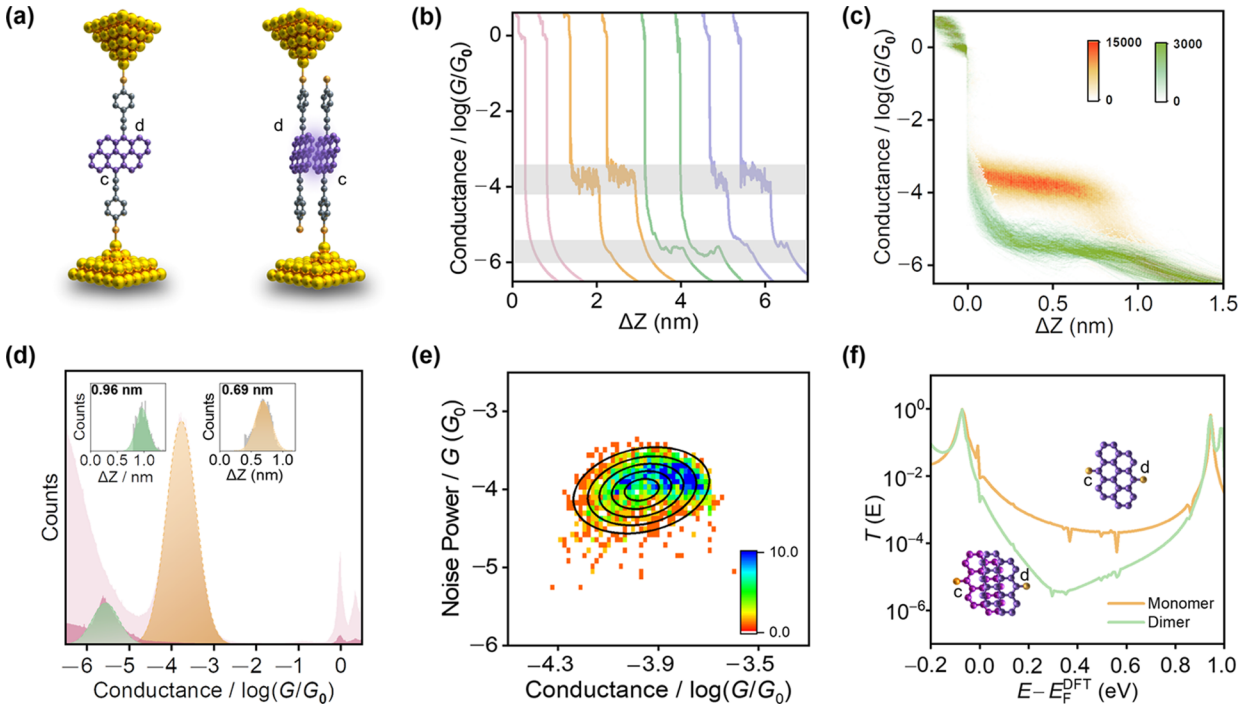

Figure 3. Charge transport of a comparative molecule CQI-H. (a) Schematic illustration of single-molecule and dimer junctions with the molecule CQI-H. (b) Typical conductance-displacement traces of background (pink), high state (yellow), low state (green), and high to low state (purple). (c) 2D conductance-displacement histograms for the molecule CQI-H at a bias of 0.1 V. The color scale shows the number of counts normalized to the number of curves included in the histograms. (d) 1D conductance histograms of the junctions in the high conductance state (yellow) and the low state (green). Inset: corresponding plateau length of separated high and low states. (e) 2D histogram of the normalized noise power versus average conductance for the high conductance state of CQI-H, calculated for 4000 measured traces. (f) Theoretical transmission spectra of a single molecule and a dimer.

which the triple bonds connect to the sites labeled as *c* and *d*. This monomer (denoted as CQI-H, a constructive QI molecule with a relatively high conductance, as shown elsewhere,[20] Figure S1-1b) exhibits CQI and possesses a higher (H) conductance than the CQI-L monomer of Figure 1b (left). This higher conductance is also evident in the experimental conductance peak near 10^{-4} G_0 shown in Figure S14, which is consistent with the theoretical transmission coefficient of Figure 3f and previous study.[20] Similarly, the PSD measurement result of this high state of the molecule CQI-H is presented in Figure 3e. The noise power scales as about $G^{1.3}$, indicating that the conductance near 10^{-4} G_0 of the molecule CQI-H is attributed to through-bond transport,[39,42,43] which corresponds to the monomer. In contrast to the molecule CQI-L, an additional conductance peak appears at ~2.5 × 10^{-6} G_0 (≈0.20 nS), which is nearly 40 times lower than that of the monomer conductance (Figure 3c). Comparison with the mid-gap theoretical transmission curve of the dimer (green curve in Figure 3f) shows that in this case, the dimer conductance is expected to be lower than the monomer conductance. Again, the ratio of the low conductance increases with increasing bias voltage (Figure S14), which supports the interpretation that the high conductance originates from the monomer state. Furthermore, the plateau length of the low conductance state is greater than that of the high conductance state (Figure 3d, inset), which is different from the molecule CQI-L with similar length (Figure S5). From the typical individual conductance-displacement traces of the molecule CQI-H, traces from the high conductance to the low conductance can also be observed (Figure 3b), which corresponds to the stretching process from a single molecule to a π-stacked dimer. This is further evidence that the low conductance of the molecule CQI-H is associated with the dimer and is consistent with the theoretical model in Figure 3f, where the molecular length of the lower conductance dimer is greater than that of a single molecule. The lower conductance of the dimer is a general feature of the theoretical calculations presented in Figure S15, which show that the dimers of the molecule CQI-H with different stacking modes do not exhibit higher conductance than the monomer.

CONCLUSIONS

In summary, we have presented a combined experimental and theoretical study of charge transport in stacked graphene-like dimers and demonstrated that their highly non-classical electrical conductance is controlled by an interplay between room-temperature quantum interference and π-π stacking. For the molecule CQI-L, the most energetically favored stacking interactions can increase the electrical conductance of the dimer by a factor of ~25 in comparison with that of the monomer. In contrast, for the molecule CQI-H, the conductance of the dimer is a factor of ~40 lower than that of the monomer. This clearly demonstrates that rational control of connectivity to molecular cores in combination with stacking interactions between their π systems offers a general route to modify and optimize charge transfer between molecules, which will invite intense research at both macroscopic and microscopic levels.

https://doi.org/10.1021/jacs.2c05909
J. Am. Chem. Soc. 2022, 144, 15689−15697

■ ASSOCIATED CONTENT

Supporting Information

The Supporting Information is available free of charge at https://pubs.acs.org/doi/10.1021/jacs.2c05909.

Supplementary information of molecules CQI-L and CQI-H; XPS characterization of the devices; experimental results of the molecule CQI-L without preassembly; bias dependent conductance measurements of the molecule CQI-L; separated experimental results of the molecule CQI-L at different biases; flicker noise experimental results of high conductance states of CQI-L and CQI-H; archetypal stacking patterns of the molecule CQI-L; AA stacking of benzenes; the magic ratio theory in the bipartite lattice; charge transport when two molecules are bound to both electrodes; transmission spectra of the molecule CQI-L based on AB2 stacking; the robustness of the molecule CQI-L with high conductance state; discussions of charge transport with increasing the central core from one benzene to eight benzenes; bias dependence of the molecule CQI-H; transmission spectra of the molecule CQI-H based on AB stacking; experimental measurements of two model systems: benzylamine (one-anchor) and 1,4-di(aminomethyl)benzene (double-anchor) (PDF)

■ AUTHOR INFORMATION

Corresponding Authors

Xuefeng Guo − *Beijing National Laboratory for Molecular Sciences, National Biomedical Imaging Center, College of Chemistry and Molecular Engineering, Peking University, Beijing 100871, P. R. China; Center of Single-Molecule Sciences, Institute of Modern Optics, Frontiers Science Center for New Organic Matter, Tianjin Key Laboratory of Micro-scale Optical Information Science and Technology, College of Electronic Information and Optical Engineering, Nankai University, Tianjin 300350, P. R. China;* orcid.org/0000-0001-5723-8528; Email: guoxf@pku.edu.cn

Chuancheng Jia − *Center of Single-Molecule Sciences, Institute of Modern Optics, Frontiers Science Center for New Organic Matter, Tianjin Key Laboratory of Micro-scale Optical Information Science and Technology, College of Electronic Information and Optical Engineering, Nankai University, Tianjin 300350, P. R. China; Beijing National Laboratory for Molecular Sciences, National Biomedical Imaging Center, College of Chemistry and Molecular Engineering, Peking University, Beijing 100871, P. R. China*; Email: jiacc@nankai.edu.cn

Colin J. Lambert − *Department of Physics, Lancaster University, Lancaster LA1 4YB, UK;* orcid.org/0000-0003-2332-9610; Email: c.lambert@lancaster.ac.uk

Wenjing Hong − *State Key Laboratory of Physical Chemistry of Solid Surfaces, College of Chemistry and Chemical Engineering, Xiamen University, Xiamen 361005, P. R. China;* orcid.org/0000-0003-4080-6175; Email: whong@xmu.edu.cn

Shi-Xia Liu − *Department of Chemistry, Biochemistry and Pharmaceutical Sciences, University of Bern, CH-3012 Bern, Switzerland;* orcid.org/0000-0001-6104-4320; Email: liu@dcb.unibe.ch

Authors

Peihui Li − *Center of Single-Molecule Sciences, Institute of Modern Optics, Frontiers Science Center for New Organic Matter, Tianjin Key Laboratory of Micro-scale Optical Information Science and Technology, College of Electronic Information and Optical Engineering, Nankai University, Tianjin 300350, P. R. China*

Songjun Hou − *Department of Physics, Lancaster University, Lancaster LA1 4YB, UK*

Bader Alharbi − *Department of Physics, Lancaster University, Lancaster LA1 4YB, UK; Department of Physics, Prince Sattam Bin Abdulaziz University, Alkharj 16278, Saudi Arabia*

Qingqing Wu − *Department of Physics, Lancaster University, Lancaster LA1 4YB, UK*

Yijian Chen − *Center of Single-Molecule Sciences, Institute of Modern Optics, Frontiers Science Center for New Organic Matter, Tianjin Key Laboratory of Micro-scale Optical Information Science and Technology, College of Electronic Information and Optical Engineering, Nankai University, Tianjin 300350, P. R. China*

Li Zhou − *Center of Single-Molecule Sciences, Institute of Modern Optics, Frontiers Science Center for New Organic Matter, Tianjin Key Laboratory of Micro-scale Optical Information Science and Technology, College of Electronic Information and Optical Engineering, Nankai University, Tianjin 300350, P. R. China*

Tengyang Gao − *State Key Laboratory of Physical Chemistry of Solid Surfaces, College of Chemistry and Chemical Engineering, Xiamen University, Xiamen 361005, P. R. China*

Ruihao Li − *State Key Laboratory of Physical Chemistry of Solid Surfaces, College of Chemistry and Chemical Engineering, Xiamen University, Xiamen 361005, P. R. China*

Lan Yang − *Center of Single-Molecule Sciences, Institute of Modern Optics, Frontiers Science Center for New Organic Matter, Tianjin Key Laboratory of Micro-scale Optical Information Science and Technology, College of Electronic Information and Optical Engineering, Nankai University, Tianjin 300350, P. R. China*

Xinyue Chang − *Center of Single-Molecule Sciences, Institute of Modern Optics, Frontiers Science Center for New Organic Matter, Tianjin Key Laboratory of Micro-scale Optical Information Science and Technology, College of Electronic Information and Optical Engineering, Nankai University, Tianjin 300350, P. R. China*

Gang Dong − *State Key Laboratory of Physical Chemistry of Solid Surfaces, College of Chemistry and Chemical Engineering, Xiamen University, Xiamen 361005, P. R. China*

Xunshan Liu − *Department of Chemistry, Biochemistry and Pharmaceutical Sciences, University of Bern, CH-3012 Bern, Switzerland; Department of Chemistry, Zhejiang Sci-Tech University, Hangzhou 310018, P. R. China;* orcid.org/0000-0003-1537-258X

Silvio Decurtins − *Department of Chemistry, Biochemistry and Pharmaceutical Sciences, University of Bern, CH-3012 Bern, Switzerland*

Complete contact information is available at: https://pubs.acs.org/10.1021/jacs.2c05909

Author Contributions

[&]P.L., S.H., and B.A. contributed equally to this work.

Notes

The authors declare no competing financial interest.

■ ACKNOWLEDGMENTS

We acknowledge primary financial support from the National Key R&D Program of China (2017YFA0204901, 2021YFA1200101, 2021YFA1200102, and 2017YFA0204902), the National Natural Science Foundation of China (22150013, 22173050, 21727806, and 21933001), the Tencent Foundation through the XPLORER PRIZE, "Frontiers Science Center for New Organic Matter" at Nankai University (63181206), the Natural Science Foundation of Beijing (2222009), and Beijing National Laboratory for Molecular Sciences (BNLMS202105). C.J.L. acknowledges financial support from the UK EPSRC through grant nos. EP/M014452/1, EP/P027156/1, and EP/N03337X/1.

■ REFERENCES

(1) Chen, H. L.; Stoddart, J. F. From Molecular to Supramolecular Electronics. *Nat. Rev. Mater.* **2021**, *6*, 804−828.
(2) Madhu, M.; Ramakrishnan, R.; Vijay, V.; Hariharan, M. Free Charge Carriers in Homo-Sorted Pi-Stacks of Donor-Acceptor Conjugates. *Chem. Rev.* **2021**, *121*, 8234−8284.
(3) Li, X.; Wu, Q.; Bai, J.; Hou, S.; Jiang, W.; Tang, C.; Song, H.; Huang, X.; Zheng, J.; Yang, Y.; Liu, J.; Hu, Y.; Shi, J.; Liu, Z.; Lambert, C. J.; Zhang, D.; Hong, W. Structure-Independent Conductance of Thiophene-Based Single-Stacking Junctions. *Angew. Chem., Int. Ed.* **2020**, *59*, 3280−3286.
(4) Kim, Y.-H.; Zhai, Y.; Lu, H.; Pan, X.; Xiao, C.; Gaulding, E. A.; Harvey, S. P.; Berry, J. J.; Vardeny, Z. V.; Luther, J. M.; Beard, M. C. Chiral-Induced Spin Selectivity Enables a Room-Temperature Spin Light-Emitting Diode. *Science* **2021**, *371*, 1129−1133.
(5) Tu, L.; Xie, Y.; Li, Z.; Tang, B. Aggregation-Induced Emission: Red and near-Infrared Organic Light-Emitting Diodes. *SmartMat* **2021**, *2*, 326−346.
(6) Li, G.; Chang, W.-H.; Yang, Y. Low-Bandgap Conjugated Polymers Enabling Solution-Processable Tandem Solar Cells. *Nat. Rev. Mater.* **2017**, *2*, 17043.
(7) Lee, J.; Jadhav, P.; Reusswig, P. D.; Yost, S. R.; Thompson, N. J.; Congreve, D. N.; Hontz, E.; Van Voorhis, T.; Baldo, M. A. Singlet Exciton Fission Photovoltaics. *Acc. Chem. Res.* **2013**, *46*, 1300−1311.
(8) Chen, H.; Zhang, W.; Li, M.; He, G.; Guo, X. Interface Engineering in Organic Field-Effect Transistors: Principles, Applications, and Perspectives. *Chem. Rev.* **2020**, *120*, 2879−2949.
(9) Li, P.; Jia, C.; Guo, X. Molecule-Based Transistors: From Macroscale to Single Molecule. *Chem. Rec.* **2021**, *21*, 1284−1299.
(10) Wang, P. Q.; Jia, C. C.; Huang, Y.; Duan, X. F. Van Der Waals Heterostructures by Design: From 1d and 2d to 3d. *Matter* **2021**, *4*, 552−581.
(11) Novoselov, K. S.; Mishchenko, A.; Carvalho, A.; Castro Neto, A. H. 2d Materials and Van Der Waals Heterostructures. *Science* **2016**, *353*, No. aac9439.
(12) Liu, Y.; Huang, Y.; Duan, X. Van Der Waals Integration before and Beyond Two-Dimensional Materials. *Nature* **2019**, *567*, 323−333.
(13) Zhao, S. Q.; Wu, Q. Q.; Pi, J. C.; Liu, J. Y.; Zheng, J. T.; Hou, S. J.; Wei, J. Y.; Li, R. H.; Sadeghi, H.; Yang, Y.; Shi, J.; Chen, Z. B.; Xiao, Z. Y.; Lambert, C.; Hong, W. J. Cross-Plane Transport in a Single-Molecule Two-Dimensional Van Der Waals Heterojunction. *Sci. Adv.* **2020**, *6*, eaba6714.
(14) Wu, Q.; Sadeghi, H.; Garcia-Suarez, V. M.; Ferrer, J.; Lambert, C. J. Thermoelectricity in Vertical Graphene-C60-Graphene Architectures. *Sci. Rep.* **2017**, *7*, 11680.
(15) Stepanov, P.; Das, I.; Lu, X.; Fahimniya, A.; Watanabe, K.; Taniguchi, T.; Koppens, F. H. L.; Lischner, J.; Levitov, L.; Efetov, D. K. Untying the Insulating and Superconducting Orders in Magic-Angle Graphene. *Nature* **2020**, *583*, 375−378.
(16) Zondiner, U.; Rozen, A.; Rodan-Legrain, D.; Cao, Y.; Queiroz, R.; Taniguchi, T.; Watanabe, K.; Oreg, Y.; von Oppen, F.; Stern, A.; Berg, E.; Jarillo-Herrero, P.; Ilani, S. Cascade of Phase Transitions and Dirac Revivals in Magic-Angle Graphene. *Nature* **2020**, *582*, 203−208.
(17) Nuckolls, K. P.; Oh, M.; Wong, D.; Lian, B.; Watanabe, K.; Taniguchi, T.; Bernevig, B. A.; Yazdani, A. Strongly Correlated Chern Insulators in Magic-Angle Twisted Bilayer Graphene. *Nature* **2020**, *588*, 610−615.
(18) Rozen, A.; Park, J. M.; Zondiner, U.; Cao, Y.; Rodan-Legrain, D.; Taniguchi, T.; Watanabe, K.; Oreg, Y.; Stern, A.; Berg, E.; Jarillo-Herrero, P.; Ilani, S. Entropic Evidence for a Pomeranchuk Effect in Magic-Angle Graphene. *Nature* **2021**, *592*, 214−219.
(19) Famili, M.; Jia, C. C.; Liu, X. S.; Wang, P. Q.; Grace, I. M.; Guo, J.; Liu, Y.; Feng, Z. Y.; Wang, Y. L.; Zhao, Z. P.; Decurtins, S.; Haner, R.; Huang, Y.; Liu, S. X.; Lambert, C. J.; Duan, X. F. Self-Assembled Molecular-Electronic Films Controlled by Room Temperature Quantum Interference. *Chem* **2019**, *5*, 474−484.
(20) Geng, Y.; Sangtarash, S.; Huang, C.; Sadeghi, H.; Fu, Y.; Hong, W.; Wandlowski, T.; Decurtins, S.; Lambert, C. J.; Liu, S. X. Magic Ratios for Connectivity-Driven Electrical Conductance of Graphene-Like Molecules. *J. Am. Chem. Soc.* **2015**, *137*, 4469−4476.
(21) Valkenier, H.; Guedon, C. M.; Markussen, T.; Thygesen, K. S.; van der Molen, S. J.; Hummelen, J. C. Cross-Conjugation and Quantum Interference: A General Correlation? *Phys. Chem. Chem. Phys.* **2014**, *16*, 653−662.
(22) Guédon, C. M.; Valkenier, H.; Markussen, T.; Thygesen, K. S.; Hummelen, J. C.; van der Molen, S. J. Observation of Quantum Interference in Molecular Charge Transport. *Nat. Nanotechnol.* **2012**, *7*, 305−309.
(23) Reznikova, K.; Hsu, C.; Schosser, W. M.; Gallego, A.; Beltako, K.; Pauly, F.; van der Zant, H. S. J.; Mayor, M. Substitution Pattern Controlled Quantum Interference in [2.2]Paracyclophane-Based Single-Molecule Junctions. *J. Am. Chem. Soc.* **2021**, *143*, 13944−13951.
(24) Stefani, D.; Weiland, K. J.; Skripnik, M.; Hsu, C.; Perrin, M. L.; Mayor, M.; Pauly, F.; van der Zant, H. S. J. Large Conductance Variations in a Mechanosensitive Single-Molecule Junction. *Nano Lett.* **2018**, *18*, 5981−5988.
(25) Caneva, S.; Gehring, P.; Garcia-Suarez, V. M.; Garcia-Fuente, A.; Stefani, D.; Olavarria-Contreras, I. J.; Ferrer, J.; Dekker, C.; van der Zant, H. S. J. Mechanically Controlled Quantum Interference in Graphene Break Junctions. *Nat. Nanotechnol.* **2018**, *13*, 1126−1131.
(26) Solomon, G. C.; Vuraweis, J.; Herrmann, C.; Wasielewski, M. R.; Ratner, M. A. Understanding Coherent Transport through Π-Stacked Systems Upon Spatial Dislocation. *J. Phys. Chem. B* **2010**, *114*, 14735−14744.
(27) Nozaki, D.; Lucke, A.; Schmidt, W. G. Molecular Orbital Rule for Quantum Interference in Weakly Coupled Dimers: Low-Energy Giant Conductivity Switching Induced by Orbital Level Crossing. *J. Phys. Chem. Lett.* **2017**, *8*, 727−732.
(28) Kiguchi, M.; Takahashi, T.; Takahashi, Y.; Yamauchi, Y.; Murase, T.; Fujita, M.; Tada, T.; Watanabe, S. Electron Transport through Single Molecules Comprising Aromatic Stacks Enclosed in Self-Assembled Cages. *Angew. Chem., Int. Ed.* **2011**, *50*, 5708−5711.
(29) Martín, S.; Grace, I.; Bryce, M. R.; Wang, C.; Jitchati, R.; Batsanov, A. S.; Higgins, S. J.; Lambert, C. J.; Nichols, R. J. Identifying Diversity in Nanoscale Electrical Break Junctions. *J. Am. Chem. Soc.* **2010**, *132*, 9157−9164.
(30) Wu, S.; Gonzalez, M. T.; Huber, R.; Grunder, S.; Mayor, M.; Schonenberger, C.; Calame, M. Molecular Junctions Based on Aromatic Coupling. *Nat. Nanotechnol.* **2008**, *3*, 569−574.
(31) Lambert, C. J. *Quantum Transport in Nanostructures and Molecules*; IoP Publishing: Bristol, 2021, 20−44, DOI: 10.1088/978-0-7503-3639-0ch7.
(32) Li, J.; Zhuang, Z.; Shen, P.; Song, S.; Tang, B. Z.; Zhao, Z. Achieving Multiple Quantum-Interfered States Via through-Space and

through-Bond Synergistic Effect in Foldamer-Based Single-Molecule Junctions. *J. Am. Chem. Soc.* **2022**, *144*, 8073−8083.
(33) Shen, P.; Huang, M.; Qian, J.; Li, J.; Ding, S.; Zhou, X. S.; Xu, B.; Zhao, Z.; Tang, B. Z. Achieving Efficient Multichannel Conductance in through-Space Conjugated Single-Molecule Parallel Circuits. *Angew. Chem., Int. Ed.* **2020**, *59*, 4581−4588.
(34) Soler, J. M.; Artacho, E.; Gale, J. D.; Garcia, A.; Junquera, J.; Ordejon, P.; Sanchez-Portal, D. The Siesta Method for Ab Initio Order-N Materials Simulation. *J. Phys. Condens. Matter* **2002**, *14*, 2745−2779.
(35) Ferrer, J.; Lambert, C. J.; García-Suárez, V. M.; Manrique, D. Z.; Visontai, D.; Oroszlany, L.; Rodríguez-Ferradás, R.; Grace, I.; Bailey, S. W. D.; Gillemot, K.; Sadeghi, H.; Algharagholy, L. A. GOLLUM: A Next-Generation Simulation Tool for Electron, Thermal and Spin Transport. *New J. Phys.* **2014**, *16*, No. 093029.
(36) Frisenda, R.; Janssen, V. A.; Grozema, F. C.; van der Zant, H. S.; Renaud, N. Mechanically Controlled Quantum Interference in Individual π-Stacked Dimers. *Nat. Chem.* **2016**, *8*, 1099−1104.
(37) Solomon, G. C.; Herrmann, C.; Vura-Weis, J.; Wasielewski, M. R.; Ratner, M. A. The Chameleonic Nature of Electron Transport through Pi-Stacked Systems. *J. Am. Chem. Soc.* **2010**, *132*, 7887−7889.
(38) Bai, J.; Daaoub, A.; Sangtarash, S.; Li, X.; Tang, Y.; Zou, Q.; Sadeghi, H.; Liu, S.; Huang, X.; Tan, Z.; Liu, J.; Yang, Y.; Shi, J.; Meszaros, G.; Chen, W.; Lambert, C.; Hong, W. Anti-Resonance Features of Destructive Quantum Interference in Single-Molecule Thiophene Junctions Achieved by Electrochemical Gating. *Nat. Mater.* **2019**, *18*, 364−369.
(39) Tang, C.; Chen, L.; Zhang, L.; Chen, Z.; Li, G.; Yan, Z.; Lin, L.; Liu, J.; Huang, L.; Ye, Y.; Hua, Y.; Shi, J.; Xia, H.; Hong, W. Multicenter-Bond-Based Quantum Interference in Charge Transport through Single-Molecule Carborane Junctions. *Angew. Chem., Int. Ed.* **2019**, *58*, 10601−10605.
(40) Liu, J.; Zhao, X.; Zheng, J.; Huang, X.; Tang, Y.; Wang, F.; Li, R.; Pi, J.; Huang, C.; Wang, L.; Yang, Y.; Shi, J.; Mao, B.-W.; Tian, Z.-Q.; Bryce, M. R.; Hong, W. Transition from Tunneling Leakage Current to Molecular Tunneling in Single-Molecule Junctions. *Chem* **2019**, *5*, 390−401.
(41) Vazquez, H.; Skouta, R.; Schneebeli, S.; Kamenetska, M.; Breslow, R.; Venkataraman, L.; Hybertsen, M. S. Probing the Conductance Superposition Law in Single-Molecule Circuits with Parallel Paths. *Nat. Nanotechnol.* **2012**, *7*, 663−667.
(42) Adak, O.; Rosenthal, E.; Meisner, J.; Andrade, E. F.; Pasupathy, A. N.; Nuckolls, C.; Hybertsen, M. S.; Venkataraman, L. Flicker Noise as a Probe of Electronic Interaction at Metal-Single Molecule Interfaces. *Nano Lett.* **2015**, *15*, 4143−4149.
(43) Garner, M. H.; Li, H.; Chen, Y.; Su, T. A.; Shangguan, Z.; Paley, D. W.; Liu, T.; Ng, F.; Li, H.; Xiao, S.; Nuckolls, C.; Venkataraman, L.; Solomon, G. C. Comprehensive Suppression of Single-Molecule Conductance Using Destructive Sigma-Interference. *Nature* **2018**, *558*, 415−419.
(44) Tang, Y.; Zhou, Y.; Zhou, D.; Chen, Y.; Xiao, Z.; Shi, J.; Liu, J.; Hong, W. Electric Field-Induced Assembly in Single-Stacking Terphenyl Junctions. *J. Am. Chem. Soc.* **2020**, *142*, 19101−19109.
(45) Kamenetska, M.; Koentopp, M.; Whalley, A. C.; Park, Y. S.; Steigerwald, M. L.; Nuckolls, C.; Hybertsen, M. S.; Venkataraman, L. Formation and Evolution of Single-Molecule Junctions. *Phys. Rev. Lett.* **2009**, *102*, No. 126803.
(46) Sangtarash, S.; Huang, C.; Sadeghi, H.; Sorohhov, G.; Hauser, J.; Wandlowski, T.; Hong, W.; Decurtins, S.; Liu, S. X.; Lambert, C. J. Searching the Hearts of Graphene-Like Molecules for Simplicity, Sensitivity, and Logic. *J. Am. Chem. Soc.* **2015**, *137*, 11425−11431.
(47) Markussen, T.; Stadler, R.; Thygesen, K. S. The Relation between Structure and Quantum Interference in Single Molecule Junctions. *Nano Lett.* **2010**, *10*, 4260−4265.
(48) Tada, T.; Yoshizawa, K. J. C. Quantum Transport Effects in Nanosized Graphite Sheets. *ChemPhysChem* **2002**, *3*, 1035−1037.
(49) Yoshizawa, K.; Tada, T.; Staykov, A. Orbital Views of the Electron Transport in Molecular Devices. *J. Am. Chem. Soc.* **2008**, *130*, 9406−9413.
(50) Lambert, C. J.; Liu, S. X. A Magic Ratio Rule for Beginners: A Chemist's Guide to Quantum Interference in Molecules. *Chem* **2018**, *24*, 4193−4201.
(51) Yoshizawa, K. An Orbital Rule for Electron Transport in Molecules. *Acc. Chem. Res.* **2012**, *45*, 1612−1621.

Recommended by ACS

Heteroatom Effects on Quantum Interference in Molecular Junctions: Modulating Antiresonances by Molecular Design
Luke J. O'Driscoll, Martin R. Bryce, *et al.*
AUGUST 02, 2021
THE JOURNAL OF PHYSICAL CHEMISTRY C
READ

Electric Field-Induced Assembly in Single-Stacking Terphenyl Junctions
Yongxiang Tang, Wenjing Hong, *et al.*
NOVEMBER 02, 2020
JOURNAL OF THE AMERICAN CHEMICAL SOCIETY
READ

Substitution Pattern Controlled Quantum Interference in [2.2]Paracyclophane-Based Single-Molecule Junctions
Ksenia Reznikova, Marcel Mayor, *et al.*
AUGUST 23, 2021
JOURNAL OF THE AMERICAN CHEMICAL SOCIETY
READ

Nonexponential Length Dependence of Molecular Conductance in Acene-Based Molecular Wires
Jesús Valdiviezo, Julio L. Palma, *et al.*
JANUARY 07, 2021
ACS SENSORS
READ

Get More Suggestions >

https://doi.org/10.1021/jacs.2c05909
J. Am. Chem. Soc. 2022, 144, 15689−15697